

# Ferroelectricity and related effects on carrier transport in type-II Weyl semimetal WTe<sub>2</sub> thin film

Chen-Huan Wu \*, Yujie Ren

School of Microelectronics, Southern University of Science and Technology, 518055 Shenzhen, China

February 27, 2024

We investigate ferroelectric polariation as well as the formation of long-range order and the carrier density distribution in type-II Weyl semimetal WTe<sub>2</sub> in  $T_d$  phase. It is been found that the metallicity and ferroelectricity can coexist in bulk WTe<sub>2</sub> which has a significant impact on the electrical transport[32], despite its large conductance. Also, our theoretical calculation and numerical simulation provide a deeper insight to the electrical structure-dependent dynamics of WTe<sub>2</sub>. Base on the two-level approximation verify that the polarization stems from uncompensated out-of-plane interband transition of the electrons, which is base on the calculations of the dipole transition moment (in both the momentum space and frequency domain), and we found that the topological character of type-II Weyl system is closely related to the electronic behaviors (like the carrier compensation) and the excitations near the Weyl cone. The anisotropy and the topologically protected spin-polarized bulk (Weyl orbit) and surface states in WTe<sub>2</sub> induce hysteresis, which exhibits potential in applications of non-volatile energy-efficient data-storage devices. Part of the properties of WTe<sub>2</sub> are also shares shared by the thermoelectric properties with other two-dimensional transition-metal dichalcogenides, like the WSe<sub>2</sub> and MoTe<sub>2</sub>.

**Introduction** As a type-II Weyl semimetal, WTe<sub>2</sub> has a  $Pm$  point group symmetry, and the inversion symmetry is broken. Such non-centrosymmetry leads to non-trivial geometric properties for the Bloch states, and allows higher-order response to external electric field which contains the components along more than one principal crystallographic direction[33, 34, 35]. WTe<sub>2</sub>, as a polar metal as well as ferroelectric material, contains an intrinsic electrical dipole moment, which does not relies on the external electric field. The  $dI/dV(V)$  and  $dV/dI(I)$  measurements in bulk WTe<sub>2</sub>[1, 2] show sweep direction dependence which indicates that the source-drain field variation generates an additional polarization current. During the ferroelectrical polarization, the spontaneous polarization vector switches between the two different orientations when the oppositely oriented electric field is applied. The key experiment for ferroelectricity is the existence of a hysteresis loop between polarization and electric field. Despite the ferromagnetism in layered T<sub>d</sub>-WTe<sub>2</sub> can coexist with the Weyl semimetal phase, in the absence of doping and defects, highly pure T<sub>d</sub>-WTe<sub>2</sub> is diamagnetic, and the M-H curves show constant linear negative slope in a large scale of magnetic field. In the absence of magnetic impurity and defects, the saturation magnetic moment is vanishingly small, and the ferromagnetic order is totally overwhelmed by the semimetallic behaviors. With broken inversion symmetry and time reversal symmetry, except the ordinary Hall effect under an external magnetic field, the anomalous Hall effect can be observed under zero magnetic field and an finite bias current, like the out-of-plane magnetization which can be generated by the bias current along  $a$ -axis[36]. As an orthorhombic noncentrosymmetric material, a vertical electric field can break the two-fold screw rotation symmetry of WTe<sub>2</sub> and generating finite Berry curvature dipole which can leads to nonlinear Hall current even in the absence of magnetic field. Recent studies also focus on coexistence of ferroelectricity and nonlinear Hall (or anomalous Hall) effects[4], which also impls the unique ferroelectric properties and the related carrier transport in WTe<sub>2</sub>.

**Discussion** Ferroelectricity as an electrical collective phenomenon, is related to the rotation of dipoles. For single layer film the dipole-dipole interaction can induces mirror charges on conducting substrate and results in out-of-plane polarization[14]. Such type of ferroelectric polarization in fre layer films is realized by interlayer charge transition through the excitations of sliding phonons which carry the electric dipoles, and this sliding ferroelectric polarization as well as the shear motion of phonon driven by thermally fluctuating force is guaranteed by the high intralayer stiffness[13] up to room temperature. The low ferroelectric switching barrier and stable sliding ferroelectric polarization make it feasible for the nanoscale polarization manipulation and electric polarization switching modulation. Except the effect of shear motion which requires thermal effect, the electric dipole moment can be modulated by applying of an external electric field. Since the ferroelectric polarization will be suppressed by the screening of conduction electrons like the metallic gates [15, 13], and such screening will destroy the electrostatic internal field formed by the long-range dipolar order as well as the electrostatic potential of ions. Also, compared to the few layer films, the bulk crystals are better in preserving the long-range dipole order[13]. While in the systems with lower dimension, the long-range dipole order is suppressed, like the few layer 2D crystals or the 1D quantum system where the thermalization effect plays a key role[16, 17].

We found that the spontaneous out-of-plane electric polarization which can be switched by applying a in-plane electric field, and a bistability behavior in resistivity is available at room temperature. The long range electrostatic

---

\*chenhuanwu1@gmail.com

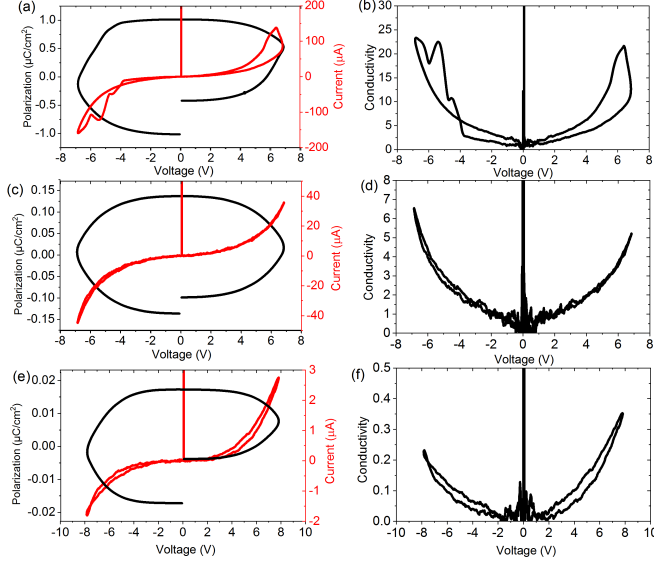


Figure 1: P-V loop measurement of 10 nm WTe<sub>2</sub> thin film using DHM method.

interaction as well as the dipole order reflects the anisotropic characteristic with the long-range Coulomb attraction for parallel dipoles along the polarization axis. Unlike the point-like Fermi surface in type-I Weyl system, there is a Fermi surface containing the electron and hole pockets of the near size. With the near electron and hole density/mobility, there are rich electrical transport phenomena, e.g., in terms of a compensated theory[21]. Also, near the contain point of the electron and hole pocktes, the out-of plane polarization in WTe<sub>2</sub> can be observed more easily ferroelectrical polarization[20] and magnetoresistivity. Furthermore, our theoretical calculation base on the two-level approximation verify that the polarization stems from uncompensated out-of-plane interband transition of the electrons, which is base on the calculations of the dipole transition moment (in both the momentum space and frequency domain), and we found that the topological character of type-II Weyl system is closely related to the electronic behaviors (like the carrier compensation) and the excitations near the Weyl cone. Though there are states from both layers in the conduction and valence bands, the cumulative effect of filled states up to the Fermi level results in a net polarization due to an imbalance of layer character, particularly near the band edges. The magnitude of this imbalance is larger for valence band states compared to the conduction band.

A slow relaxation process and the dependence on sign of current change was previously reported at room temperature[10]. This conclusion is also confirmed by gate voltage dependencies, so our results can be understood as a direct demonstration of the ferroelectric behavior of WTe<sub>2</sub> in charge transport experiment. For the ferroelectric polarization of thin film WTe<sub>2</sub>, the DHM measurement is applied to study by gate voltage dependence the polarization reversal. Similar to the above mentioned experimental results, the second-order effect here is still depends on the certain crystal axis due to the in-plane anisotropy of WTe<sub>2</sub>.

**Experimental results** Different to the semiconductor ferroelectricity, the effect of band bending caused by polarized bound charges in channel can be ignored, and instead, we have to consider the effect of mobile charges, which play a essential role in ferroelectric performance and exhibit difference in large and low current cases. We found that, at low current ( $< 1\mu A$ ), the polarization is quite small,  $\sim 0.0035 \mu C/cm^2$  for ten-layer WTe<sub>2</sub>, and the current is mainly dominated by the polarization current but the leakage current has a higher sensitivity on the voltage as well as the sweeping direction.

The interlayer charge transfer of mobile carriers has an impact on the out-of-plane polarization up to 10-20 layers, where the electric field-switchable polarization could be as large as  $1 \mu C/cm^2$  for maximal current  $\sim 100 \mu A$  and channel length up to  $40\mu m$ . Polarization states in conductivity as well as the large polarization is more easy to realized with small current. Under small current, the polarization decrease more rapidly with the decreasing current than that under high current along the channel, and the two polarization states can be revealed by the conductivity. This prove the switching capability of WTe<sub>2</sub> up to dozens of layers.

We found that, for current (or conductivity) nonzero in both the positive and negative voltages, the P-V loop exhibit circular shape, which is similar to the high frequency result of 10-nm thick HZO film[37], and the value of polarization is relatively large. In both cases, the two polarization states can be observed in conductivity.

As shown in Fig.2, the effect of large leakage current, which is triggered by the largest voltage that each sweeping would reaches at, is more significant (compares to the polarization current) for the sweeping direction from large voltage toward zero. Meanwhile the polarization-bound charge is hard to maintained due to the metallicity which destroy the upward built-in electric field (by the mobile charge) in channel. Such critical value for the dominating leakage current is weakly asymmetry with respect to the voltage, and results in different current response to the positive and negative voltage. Furthermore, the polarization in WTe<sub>2</sub> becomes more sensitive to the length of channel, where the polarization field as well as the upward built-in electric field totally suppressed by the electric field along the channel, in which case the delocalization of carrier plays the main role and the polariation states can nearly no longer be found.

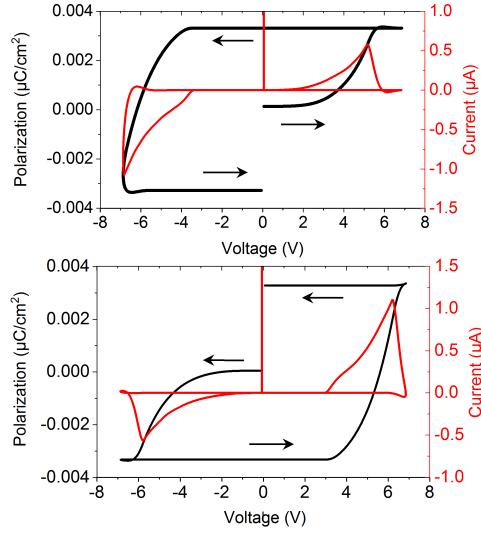


Figure 2: Ferroelectroc performance at low current realized by higher frequency. With increasing voltage, there is a accumulation of voltage pulses that results in the strengthen of ferroelectric polarization. But it is a short-term potentiation with volatile polarization. The arrows indicate the sweeping direction.

*Conclusion* There is significant role for the semimetal charge transport in the related phenomenons, especially at nearly equal hole and electron densities. Except the experimental observation, we theoretically consider the highly anisotropic electronic structure near the type-II Weyl cone of  $\text{WTe}_2$  in terms of the low-energy two band model. The calculation of dipole transition matrix element exhibit great different to other Dirac or Weyl (like the type-I) low-dimensional materials, which is due to its nearly compensated fermi surface and the anisotropic response to the magnetic field. Except the electrical anisotropy as well as the outstanding out-of-plane ferroelectricity, the calculation of dipole (modelled using a one-dimensional effective external field) can also explain the special pattern of the resonance in semimetal charge transport which is different to that in other materials with saturating magnetoresistivity[26]. Considering the interband contributions, we calculation, in terms of dipole transition, the anisotropic electrical response to external field. Hysteresis originates from ferroelectric polarization also observed through the hysteresis loop of the out-of-plane polarization.

## Appendix

### Analytical calculations and numerical simulations

In the presence of SOC, there are not Weyl nodes at  $k_z \neq 0$ [8], and the tilting is along the  $k_y$  direction ( $b$ -axis of WTe<sub>2</sub>), which makes the chiral photocurrent response originating from different tilting of Weyl cones is impossible to exist for a normally incident light. Such a chiral photocurrent is possible only by a circularly polarized light which could induce spin-flipping and be irradiated along the tilting direction ( $b$ -axis), due to the intrinsic noncentrosymmetry properties where both the time-reversal symmetry and inversion symmetry are broken. Although the inversion symmetry is absent in Weyl semimetal WTe<sub>2</sub>, the in-plane two-fold rotational symmetry is preserved[27] as indicated by the mirror symmetry plane  $\mathcal{M}_{yz}$  and glide mirror symmetry plane  $\mathcal{M}_{xz}$ . This in-plane symmetry will lead to cancellation of any in-plane optical response induced by normally-incident circularly-polarized light. Thus the nonlinear AC photoconductivity tensors are vanishingly small other than the  $\chi_{zxx}$  and  $\chi_{zyy}$  (which are directly related to the induced current in  $z$ -direction which does not affect by the twofold rotational symmetry), based on the experimentally obtained WTe<sub>2</sub> band structure near a Weyl cone. Such an in-plane response cancellation will vanish for third-order Harmonic generation. Similarly, the chiral anomaly-induced linear or nonlinear Hall current is only possible to be realized by a pair of non-orthogonal magnetic field and electric field[27], applied in the direction of tilting. Thus a vertical magnetic field can still be applied to enhance the electron interactions. That is also why we consider only one Weyl node, as the internode scattering or the internode current (like chiral anomaly) are absent without the strong magnetic field or light field along  $b$ -axis. Another difference to the photocurrent process is that, for circularly polarized light-driven photocurrent, the excitation usually has a long relaxation time due to the large weight of optical absorption which may even increase for larger layer number and thus reduce the SHG intensity. The enhancement of circular photogalvanic effect, can effectively suppress the optical absorption by reducing the relaxation time for a perturbed electron back to equilibrium.

For materials lacking the inversion symmetry like MoS<sub>2</sub>, hBN, and 1T<sub>d</sub> WTe<sub>2</sub>, the nonlinear effects like the SHG or HHG are available without needing a material junction or bias voltage. As a low-symmetry two-dimensional semimetal, WTe<sub>2</sub> is also a promising candidate for the nonlinear effect, like the current-induced SHG through the applying a bias or gate voltage, and the circular photovoltage response. During these explorations, it is vital in keeping the equilibrium distribution of electrons. For example, by selecting a proper low-frequency of light (at near-infrared range and satisfying the optical resonance), we can greatly avoid the optical absorption as well as the off-resonance excitations, which is a linear response and can be enhanced by increasing layer number of WTe<sub>2</sub> and thus suppresses the SHG. Besides, the optical absorption is possibly leads to photodamages. For WTe<sub>2</sub> in  $T_d$  phase which is noncentrosymmetric, its two-fold rotational symmetry with a mirror plane  $\mathcal{M}_{yz}$  and a glide mirror plane  $\mathcal{M}_{xz}$  results in an in-plane inversion symmetry, and thus leads to the cancellation of any in-plane components of photocurrent induced by a normally incident circularly polarized light. When considering the spin and Weyl cone tilting, there is actually a compound symmetry comprising both the time-reversal and two-fold rotation where the time-reversal process here has two effects: reverse the tilting direction and flip the spin. Experimental result[31] shows that for WTe<sub>2</sub> under obliquely incident light, the in-plane nonzero polarization-dependent current is only possible in the presence of a  $z$  polarization, while the in-plane nonzero spin current is only possible in the presence of nonzero electromagnetic potential components in three directions, i.e., the propagating direction of photon cannot be parallel to any crystal axes. Thus for a normally incident light, we can efficiently avoid the disturbances from in-plane photocurrents. As a response to the source-drain field variation, the ferroelectric polarization can be induced even by a dc electric current applied along the  $a - b$  surface of WTe<sub>2</sub>, and this can be understood as an excitation to a state that containing more out-of-plane (vertical) polarization, in addition to the spontaneous polarization due to the lack of inversion symmetry. Similar polarization effect can be seen from the magnetic-sweeping -direction dependence of the Hall resistivity at low-temperature limit.

### Tight-binding model analysis

For WTe<sub>2</sub>, there are four pairs of Weyl points in the  $k_z = 0$  plane, and each containing two Weyl points with opposite chiralities[8]. For most Dirac/Weyl systems, the energy dispersion is linear along the primary rotation axis, and be linear, higher in power for the in-plane directions. For Weyl system the power of in-plane dispersion corresponds to the account of degenerated conventional Weyl fermions with the same chirality. Specifically, to ensuring the Weyl point be of type-II, along the primary axis, it must satisfy that the electron and hole pockets are touched and the kinetic energy is dominant compared the potential energy. Also, a vector-like potential behavior and the chiral zero mode (the so-called chiral anomaly) only appear when the direction of the in-plane magnetic field is within this range. For WTe<sub>2</sub>, this direction is roughly along the direction of  $b$ -axis, where there is a Weyl nodal line connecting two Weyl points with opposite chiralities. We use the location of one of the in-plane Weyl points reported in Ref.[8], which is  $(k_x, k_y) = (0.1241, 0.0454) \text{ eV}\text{\AA}$ . While another Weyl point is at  $(k_x, k_y) = (0.12184, 0.03825)$ , then the direction of magnetic field validating the chiral anomaly  $\tan \theta = \frac{k_y}{k_x} \leq -3.8$  or  $\tan \theta = \frac{k_y}{k_x} \geq 0.55$ . According to the experiments conducted in this work, we further explore the different effects brought by the magnetic field or electric current along different in-plane directions of the WTe<sub>2</sub> bulk crystal sample in  $T_d$  phase. This also reveals the anisotropic structure of the WTe<sub>2</sub>. Due to the anisotropic Fermi surface, which results in the magnetic field selection for the chiral anomaly, WTe<sub>2</sub> displays a different degree of non-saturating magnetoresistivity and electron-hole compensation. Along  $b$ -axis which is dominated by the kinetic term and just within the Weyl cone, the effect of compensated Fermi surfaces as well as the Weyl electronic structure is much lighter than that in the other directions. While the electron-hole compensation is essential in non-saturating magnetoresistivity, the direction where chiral anomaly could be found may exhibit stronger dependence on the multiband effect (larger overlap between the valence band and conduction band).

For general Weyl semimetals, we consider the following Hamiltonian

$$H = \chi \varepsilon_0 (k_x \sigma_x + k_y \sigma_y + k_z \sigma_z) - \mu \sigma_0, \quad (1)$$

where in a lattice model  $\varepsilon_0 = \hbar v = ta$  where  $t$  is the hopping integral and  $a$  is the lattice constant. For such linearized Hamiltonian, the generalized derivatives  $v_{mn}^{ab}$  can be ignored. For convenience in calculation, we use the following coordinate transformation

$$\begin{aligned} k_x &= \rho \sin\theta \cos\phi, \\ k_y &= \rho \sin\theta \sin\phi, \\ k_z &= \rho \cos\theta. \end{aligned} \quad (2)$$

Thus we have

$$dk_x dk_y dk_z = \rho^2 \sin\theta d\rho d\theta d\phi, \quad (3)$$

and the eigenvalues of the above Hamiltonian reads  $\varepsilon_{m=0,1} = -\mu \pm \chi\rho$  for a two-band model. Then the velocity operators  $v^a$  can be obtained as

$$\begin{aligned} v^x &= \chi \begin{pmatrix} \cos 2\theta \csc\theta \sec\theta \sec\phi & (1 + i \cot\phi)(-2i + \cot\phi)\tan\phi \\ (1 - i \cot\phi)(2i + \cot\phi)\tan\phi & -\cos 2\theta \csc\theta \sec\theta \sec\phi \end{pmatrix}, \\ v^y &= \chi \begin{pmatrix} \cos 2\theta \csc\theta \csc\phi \sec\theta & -3i + 2\cot\phi - \tan\phi \\ 3i + 2\cot\phi - \tan\phi & -\cos 2\theta \csc\theta \csc\phi \sec\theta \end{pmatrix}, \\ v^z &= \chi \begin{pmatrix} 2 & \cos 2\theta \csc\theta \sec\theta(-\cos\phi + i \sin\phi) \\ \cos 2\theta \csc\theta \sec\theta(-\cos\phi - i \sin\phi) & -2 \end{pmatrix}, \end{aligned} \quad (4)$$

and the matrix elements can be obtained as

$$\begin{aligned} v_{mn}^x &= \langle m | v^x | n \rangle \\ &= \delta_{mn} \langle v^x \rangle \left( \frac{k_x}{\rho} \right) (-\delta_{m,0} + \delta_{m,1}) + (1 - \delta_{mn}) \langle v^x \rangle \left( \frac{k_z}{\rho} \frac{k_x}{\sqrt{k_x^2 + k_y^2}} - i \frac{k_y}{\sqrt{k_x^2 + k_y^2}} \right) \\ &= \delta_{mn} \langle v^x \rangle (\sin\theta \cos\phi) (-\delta_{m,0} + \delta_{m,1}) + (1 - \delta_{mn}) \langle v^x \rangle (\cos\theta \cos\phi - i \sin\phi), \\ v_{mn}^y &= \delta_{mn} \langle v^y \rangle (\sin\theta \sin\phi) (-\delta_{m,0} + \delta_{m,1}) + (1 - \delta_{mn}) \langle v^y \rangle (\cos\theta \sin\phi - i \cos\phi), \\ v_{mn}^z &= \delta_{mn} \langle v^z \rangle \cos\theta (-\delta_{m,0} + \delta_{m,1}) + (1 - \delta_{mn}) \langle v^z \rangle \frac{-\sin\theta}{\rho}, \end{aligned} \quad (5)$$

where the additional term  $(-\delta_{m,0} + \delta_{m,1})$  consider the two-band model in which case the intraband velocity depends on the band index  $m, n = 0, 1$ .  $\langle v^a \rangle$  denotes the eigenvalues of matrix  $v^a$ .

When the effect of spin-orbit coupling is considered, there are gapless Weyl nodes in type-II Weyl semimetal WTe<sub>2</sub>. Similar to graphene, when the electron move from the linear valence band to the linear conduction band near a Weyl node, or vice versa, there will be a strong instantaneous acceleration when the electron close the node, and leads to strong emission of detectable radiation in the mean time. That means the electrical dipole effect considered during this process mostly comes from the interband transition, the electron will turning back to the equilibrium position after the perturbation. But the broaden peak at finite temperature implies the existence of relaxations, due to, e.g., the impurity or phonon scatterings.

For WTe<sub>2</sub> in  $Pmn2_1$  space group, both the time-reversal symmetry and the inversion symmetry are broken, which give rise to nonzero Berry curvature. When the spin-orbit coupling (SOC) is being considered to make the interband transition is possible[8], the layer number indeed affects littlely on the band structure as well as the valence band SOC splitting[29] of WTe<sub>2</sub>. Next we using the experimentally obtained parameters of Ref.[8], where the Hamiltonian of type-II Weyl semimetal WTe<sub>2</sub> reads

$$H = Ak_x \sigma_0 + Bk_y \sigma_0 + ak_x \sigma_y + bk_x \sigma_z + dk_y \sigma_z + ek_z \sigma_x, \quad (6)$$

with  $A = -2.7, B = 0.6, a = 1, b = 1.1, d = 0.27, e = 0.184$ . Following the above coordinate transformation, the matrix form of the Hamiltonian is

$$H = \begin{pmatrix} (A\rho + b\rho)\cos\phi\sin\theta + (B\rho + d\rho)\sin\phi\sin\theta & e\rho\cos\theta - i a \rho \cos\phi \sin\theta \\ e\rho\cos\theta + i a \rho \cos\phi \sin\theta & (A\rho - b\rho)\cos\phi\sin\theta + (B\rho - d\rho)\sin\phi\sin\theta \end{pmatrix}. \quad (7)$$

After substituting the above parameters, we obtain the eigenvalue of the Hamiltonian as  $\varepsilon_+ = 1.06\rho\hbar v_0$  for the conduction band, and  $\varepsilon_- = 0.7\rho\hbar v_0$  for valence band. Here we select the points at  $|k| = ta$  away from the Weyl node, and setting the chemical potential as  $\mu \approx (\varepsilon_+ + \varepsilon_-)/2$  to prevent the optical absorption when the incoming photon energies is higher than the band gap. Thus for WTe<sub>2</sub>, by turning the chemical potential to  $\mu = \rho\hbar v_0$ , we redefine the energies of the three levels as  $\varepsilon_m = -0.3\rho\hbar v_0, \varepsilon_n = -0.15\rho\hbar v_0, \varepsilon_l = 1.06\rho\hbar v_0$ . Both of these two energies are positive, indicating that one of them is electron band while the other is hole band, with the same topologically protected chirality.

Since the type-II Weyl point requires kinetic energy dominates[8], and thus  $\phi$  should be in the range  $0.58\pi > \phi > \pi/2$  or  $1.58\pi > \phi > 3\pi/2$ . In this case, through the same procedure shown in above and by taking  $\phi = 0.55\pi$ , we obtain the eigenvalues of velocity operators as  $\langle v_x \rangle \approx -12.3\varepsilon_0/\hbar, \langle v_y \rangle \approx -4.9\varepsilon_0/\hbar$  and  $\langle v_z \rangle \approx 0.75\varepsilon_0/\hbar$ .

#### *Electrical dipole transition moment in two level approximation*

The ferroelectric switching as well as the polarization for low-symmetry ferroelectric material is closely related to the electrically tunable spontaneous dipole, like the long range electrostatic interaction and the surface dipoles which can be modulated by the interlayer shear displacement[12]. In this section, we using the two level approximation in the semiclassical framework to discuss the electrical dipole in bulk WTe<sub>2</sub> as well as its effect on the ferroelectric polarization. The dipole transition provides a way to study the low-energy excitations around the type-II Weyl point, in terms of a

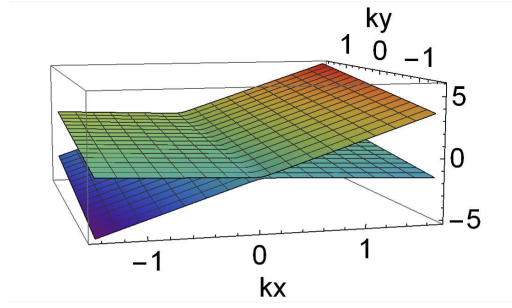


Figure 3: Band structure of WTe<sub>2</sub> near the Weyl node located at  $(k_x, k_y) = (0.1241, 0.0454)$ . We show the region of  $(0.1241 \pm \pi/2, 0.0454 \pm \pi/2)$  in momentum space.

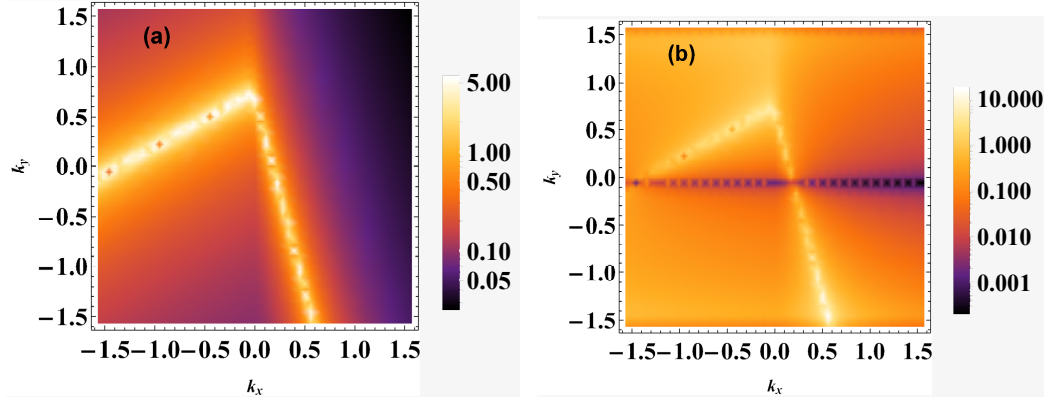


Figure 4: Real part (a) and imaginary part (b) of the interband dipole with electric field at frequency  $\omega = 0$ .

two-level approximation. We mainly consider the dipole along the  $k_y$ -direction in the  $k_z = 0$  plane, where there is a part of Chern number with opposite sign. In term our theoretical model, the possibility to modify the electron-hole correlation near the Fermi surface (contains the electron and hole pocket) by applying an in-plane electric field is further confirmed.

The perfect charge compensation (comparable electron and hole concentrations) in WTe<sub>2</sub> allows the usage of two-level approximation here. According to the parameter in Ref.[8], we consider one of the Weyl cone in  $x - y$  plane within the first Brillouin zone, where the relativistic Weyl fermions are described by the dispersion

$$\varepsilon_{\pm} = 1.204k_x + 0.686k_y \pm \sqrt{(-1.159k_x)^2 + (1.046k_x + 0.055k_y)^2}, \quad (8)$$

where the Weyl point is located in  $(k_x, k_y) = (0.1241, 0.0454)$ , and here a local stable region near the Weyl node with a point-like degeneracy is restricted by the range  $k_x^2 + k_y^2 = 10^{-6}$ [8]. As a superposition of the superposition of eigenstates, the wavefunction reads

$$\Psi(t, \mathbf{r}) = \frac{1}{N} \sum_{\mathbf{k} \in \text{BZ}} \left( \sum_n u_n(\mathbf{k}, \mathbf{r}) \phi_n(\mathbf{k}, t) + \sum_m u_m(\mathbf{k}, \mathbf{r}) \phi_m(\mathbf{k}, t) \right), \quad (9)$$

where  $u_n(\mathbf{k}, \mathbf{r})$  and  $u_m(\mathbf{k}, \mathbf{r})$  are the periodic part of the Bloch wave functions.

For arbitrary  $\alpha$ , we have  $\cos\theta_k = e^{2i\mathbf{k}\cdot\mathbf{r}} - 1$  which directly determines the energy dispersion, thus the in the dipole transition process, the transition frequency reads  $|\varepsilon_n - \varepsilon_m| = \Delta_0 \cos^{-1}\theta_k$  where  $\Delta_0$  is the momentum-independent

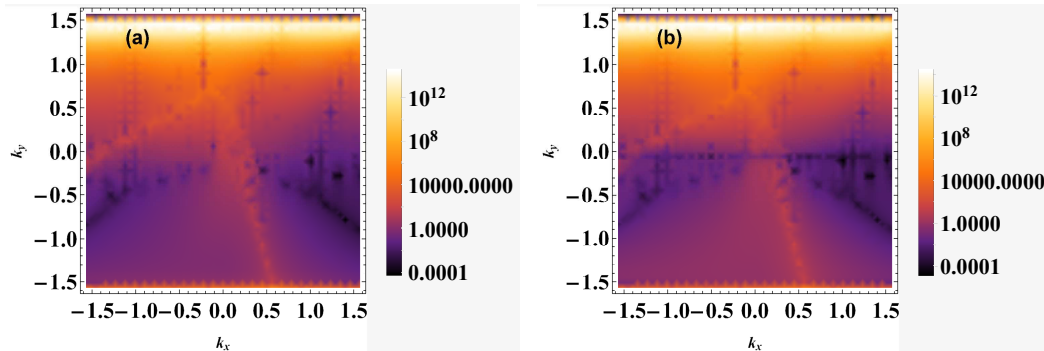


Figure 5: The same with Fig.4 but with field frequency  $\omega = \pi$ .



free electron energy (the free particle kinetic energy which can be viewed as a constant here), and considering the classical saddle point analysis, the effective action can be obtained from the transition frequency in time domain as  $S(k, t, t') = \int_{t'}^t d\tau |\varepsilon_n - \varepsilon_m|(\tau)$ . In terms of the (interband) transition dipole, we consider the hopping integral as  $f(k) = -2 \cos k_x - 2 \cos k_y + 2i \sin k_x + 2i \sin k_y$ , and the dipole matrix element reads  $D(k) = \langle u_n(k, \mathbf{r}) | \mathbf{r} | u_m(k, \mathbf{r}) \rangle = \frac{1}{2} \partial_k \psi(k)$ . The non-adiabatic type coupling can be regarded as originates from the dynamics of the mixing angle, i.e.,  $\dot{\theta}_k$ . Before substitution, the set of TDSE reads

$$\begin{aligned} E\phi_n(k) &= (E_n(k) - E(t)D_{nm} - iE(t)\partial_k)\phi_n(k) - \frac{E(t)}{2}\partial_k\psi_k\phi_m(k), \\ E\phi_m(k) &= (E_m(k) - E(t)D_{nm} - iE(t)\partial_k)\phi_m(k) - \frac{E(t)}{2}\partial_k\psi_k\phi_n(k), \end{aligned} \quad (10)$$

Considering the linearly polarized electric field, we have

$$\begin{aligned} E\phi_n(k) &= (E_n(k) - E(t)D_x(k_y) - iE(t)\frac{\partial}{\partial k_x})\phi_n(k) - \frac{E(t)}{2}\partial_{k_x}\psi_k\phi_m(k), \\ E\phi_m(k) &= (E_m(k) - E(t)D_x(k_y) - iE(t)\frac{\partial}{\partial k_x})\phi_m(k) - \frac{E(t)}{2}\partial_{k_x}\psi_k\phi_n(k), \\ E\phi_n(k) &= (E_n(k) - E(t)D_y(k_x) - iE(t)\frac{\partial}{\partial k_y})\phi_n(k) - \frac{E(t)}{2}\partial_{k_y}\psi_k\phi_m(k), \\ E\phi_m(k) &= (E_m(k) - E(t)D_y(k_x) - iE(t)\frac{\partial}{\partial k_y})\phi_m(k) - \frac{E(t)}{2}\partial_{k_y}\psi_k\phi_n(k), \end{aligned} \quad (11)$$

with the solved coefficients

$$\begin{aligned} \phi_n(k_x) &= A_1 \text{Exp} \left[ -\frac{i}{E(t)} [Ek_x - \int_0^{k_x} [E_n - E(t)D_x(k_y)] dk_y] \right], \\ \phi_m(k_x) &= A_2 \text{Exp} \left[ -\frac{i}{E(t)} [Ek_x - \int_0^{k_x} [E_m - E(t)D_x(k_y)] dk_y] \right], \\ \phi_n(k_y) &= A_3 \text{Exp} \left[ -\frac{i}{E(t)} [Ek_y - \int_0^{k_y} [E_n - E(t)D_y(k_x)] dk_x] \right], \\ \phi_m(k_y) &= A_4 \text{Exp} \left[ -\frac{i}{E(t)} [Ek_y - \int_0^{k_y} [E_m - E(t)D_y(k_x)] dk_x] \right]. \end{aligned} \quad (12)$$

It shows that only the  $\phi_n(k_x)$  and  $\phi_m(k_y)$  be the reasonal results due to the special form of 1D dipoles  $D_x(k_y)$  and  $D_y(k_x)$ . Using the dipole transition matrix elements and according to Larmor semiclassical theory, the low-energy excitation around type-II Weyl point due to the dipole acceleration can be obtained by considering the following interband contribution  $\mathbf{d}(t) = \int dk D(k)(\phi_n(k, t)\phi_m^*(k, t) + h.c.)$ .

## References

- [1] Orlova N N, Ryshkov N S, Timonina A V, et al. Evidence of the ferroelectric polarization in charge transport through WTe<sub>2</sub> Weyl semimetal surface[J]. JETP Letters, 2021, 113(6): 389-395.
- [2] Orlova N N, Timonina A V, Kolesnikov N N, et al. Current-induced control of the polarization state in a polar-metal-based heterostructure SnSe/WTe<sub>2</sub>[J]. Europhysics Letters, 2022, 138(2): 26002.
- [3] Nandy S, Zeng C, Tewari S. Chiral anomaly induced nonlinear Hall effect in semimetals with multiple Weyl points[J]. Physical Review B, 2021, 104(20): 205124.
- [4] Wang H, Qian X. Ferroelectric nonlinear anomalous Hall effect in few-layer WTe<sub>2</sub>[J]. npj Computational Materials, 2019, 5(1): 1-8.
- [5] Kang K, Li T, Sohn E, et al. Nonlinear anomalous Hall effect in few-layer WTe<sub>2</sub>[J]. Nature materials, 2019, 18(4): 324-328.
- [6] Morimoto, T. Nagaosa, N. Chiral anomaly and giant magnetochiral anisotropy in noncentrosymmetric Weyl semimetals. Phys. Rev. Lett. 117, 146603 (2016).
- [7] Wang, H. Qian, X. Ferroicity-driven nonlinear photocurrent switching in timereversal invariant ferroic materials. Sci. Adv. 5, eaav9743 (2019).
- [8] na, Gresch D, Wang Z, et al. Type-II weyl semimetals[J]. Nature, 2015, 527(7579): 495-498.
- [9] Tiwari A, Chen F, Zhong S, et al. Giant c-axis nonlinear anomalous Hall effect in Td-MoTe<sub>2</sub> and WTe<sub>2</sub>[J]. Nature communications, 2021, 12(1): 1-8.
- [10] Orlova N N, Ryshkov N S, Timonina A V, et al. Evidence of the ferroelectric polarization in charge transport through WTe<sub>2</sub> Weyl semimetal surface[J]. JETP Letters, 2021, 113(6): 389-395.
- [11] Wang L, Gutiérrez-Lezama I, Barreteau C, et al. Tuning magnetotransport in a compensated semimetal at the atomic scale[J]. Nature communications, 2015, 6(1): 8892.

- [12] Ni Z, Minamitani E, Kawahara K, et al. Mechanically tunable spontaneous vertical charge redistribution in few-layer WTe<sub>2</sub>[J]. The Journal of Physical Chemistry C, 2019, 124(3): 2008-2012.
- [13] Tang P, Bauer G E W. Sliding Phase Transition in Ferroelectric van der Waals Bilayers[J]. Physical Review Letters, 2023, 130(17): 176801.
- [14] Duan C, Mei W N, Yin W G, et al. Simulations of ferroelectric polymer film polarization: The role of dipole interactions[J]. Physical Review B, 2004, 69(23): 235106.
- [15] Sharma P, Xiang F X, Shao D F, et al. A room-temperature ferroelectric semimetal[J]. Science advances, 2019, 5(7): eaax5080.
- [16] Li W, Qian X, Li J. Phase transitions in 2D materials[J]. Nature Reviews Materials, 2021, 6(9): 829-846.
- [17] Wu C H. Statistic behaviors of gauge-invariance-dominated 1D chiral current random model[J]. arXiv preprint arXiv:2207.07821, 2022.
- [18] Yang H C, Liu S H, Wang L M, et al. Longitudinal and transverse Hall resistivity of epitaxial SrRuO<sub>3</sub> films[J]. Journal of applied physics, 1999, 85(8): 5792-5794.
- [19] Parker D E, Morimoto T, Orenstein J, et al. Diagrammatic approach to nonlinear optical response with application to Weyl semimetals[J]. Physical Review B, 2019, 99(4): 045121.
- [20] Fei Z, Zhao W, Palomaki T A, et al. Ferroelectric switching of a two-dimensional metal[J]. Nature, 2018, 560(7718): 336-339.
- [21] Pletikosic I, Ali M N, Fedorov A V, et al. Electronic structure basis for the extraordinary magnetoresistance in WTe<sub>2</sub>[J]. Physical review letters, 2014, 113(21): 216601.
- [22] Guan M X, Wang E, You P W, et al. Manipulating Weyl quasiparticles by orbital-selective photoexcitation in WTe<sub>2</sub>[J]. Nature Communications, 2021, 12(1): 1885.
- [23] Majhi K, Kakani V, Ganesan R, et al. Signature of Lifshitz transition in WTe<sub>2</sub>. 08 nanosheets detected through electrical transport measurements[J]. Applied Physics Letters, 2022, 120(9): 093105.
- [24] Fei Z, Palomaki T, Wu S, et al. Edge conduction in monolayer WTe<sub>2</sub>[J]. Nature Physics, 2017, 13(7): 677-682.
- [25] Woods J M, Shen J, Kumaravadivel P, et al. Suppression of magnetoresistance in thin WTe<sub>2</sub> flakes by surface oxidation[J]. ACS applied materials interfaces, 2017, 9(27): 23175-23180.
- [26] Ali M N, Xiong J, Flynn S, et al. Large, non-saturating magnetoresistance in WTe<sub>2</sub>[J]. Nature, 2014, 514(7521): 205-208.
- [27] Li P, Zhang C, Wen Y, et al. Anisotropic planar Hall effect in the type-II topological Weyl semimetal WTe<sub>2</sub>[J]. Physical Review B, 2019, 100(20): 205128.
- [28] Du Z Z, Wang C M, Lu H Z, et al. Band signatures for strong nonlinear Hall effect in bilayer WTe<sub>2</sub>[J]. Physical Review Letters, 2018, 121(26): 266601.
- [29] Liu G B, Xiao D, Yao Y, et al. Electronic structures and theoretical modelling of two-dimensional group-VIB transition metal dichalcogenides[J]. Chemical Society Reviews, 2015, 44(9): 2643-2663.
- [30] Panday S R, Fregoso B M. Strong second harmonic generation in two-dimensional ferroelectric IV-monochalcogenides[J]. Journal of Physics: Condensed Matter, 2017, 29(43): 43LT01.
- [31] Lim S, Rajamathi C R, Sü? V, et al. Temperature-induced inversion of the spin-photogalvanic effect in WTe<sub>2</sub> and MoTe<sub>2</sub>[J]. Physical Review B, 2018, 98(12): 121301.
- [32] Sharma, Pankaj, et al. "A room-temperature ferroelectric semimetal." Science advances 5.7 (2019): eaax5080.
- [33] Ortix, Carmine. "Nonlinear Hall Effect with Time-Reversal Symmetry: Theory and Material Realizations." Advanced Quantum Technologies 4.9 (2021): 2100056.
- [34] Deb, Swarup, et al. "Cumulative polarization in conductive interfacial ferroelectrics." Nature 612.7940 (2022): 465-469.
- [35] Zhou, Yaoqiang, et al. "Contact-engineered reconfigurable two-dimensional Schottky junction field-effect transistor with low leakage currents." Nature communications 14.1 (2023): 4270.
- [36] Kang, Kaifei, et al. "Switchable moiré potentials in ferroelectric WTe<sub>2</sub>/WSe<sub>2</sub> superlattices." Nature Nanotechnology (2023): 1-6.
- [37] Gao, Zhaomeng, Shuxian Lyu, and Hangbing Lyu. "Frequency dependence on polarization switching measurement in ferroelectric capacitors." Journal of Semiconductors 43.1 (2022): 014102.